

Resilience of Hund’s rule in the Chemical Space of Small Organic Molecules

Atreyee Majumdar and Raghunathan Ramakrishnan*

¹Tata Institute of Fundamental Research, Hyderabad 500046, India

(Dated: May 7, 2024)

We embark on a quest to identify small molecules in the chemical space that can potentially violate Hund’s rule. Utilizing twelve TDDFT approximations and the ADC(2) many-body method, we report the energies of S_1 and T_1 excited states of 12,880 closed-shell organic molecules within the bigQM7 ω dataset with up to 7 CONF atoms. In this comprehensive dataset, none of the molecules, in their minimum energy geometry, exhibit a negative S_1 - T_1 energy gap at the ADC(2) level while several molecules display values < 0.1 eV. The spin-component-scaled double-hybrid method, SCS-PBE-QIDH, demonstrates the best agreement with ADC(2). Yet, at this level, a few molecules with a strained sp^3 -N center turn out as false-positives with the S_1 state lower in energy than T_1 . We investigate a prototypical cage molecule with an energy gap < -0.2 eV, which a closer examination revealed as another false positive. We conclude that in the chemical space of small closed-shell organic molecules, it is possible to identify geometric and electronic structural features giving rise to S_1 - T_1 degeneracy; still, there is no evidence of a negative gap. We share the dataset generated for this study as a module, to facilitate seamless molecular discovery through data mining.

I. INTRODUCTION

Studies from the 1970s onward, some even titled “Violation of Hund’s (multiplicity) rule...” have explored the possibility of an electronic state of lower spin-multiplicity being more stable than its higher multiplicity counterpart [1–7]. Although no experimentally known cases of Hund’s rule violation exist among molecules in their ground state, *ab initio* wavefunction models have suggested that dynamic spin polarization effects may favor open-shell singlets over triplets[1]. In 1980, Leupin *et al.* suggested the likelihood of a more stable lowest excited singlet state, S_1 , compared to the triplet state, T_1 , based on fluorescence measurements of cycl[3.3.3]azines[8]. Likewise, in 1985, certain non-alternant polycyclic hydrocarbons were considered to exhibit negative S_1 - T_1 gaps (STGs)[2]. Typically, S_1 and T_1 are represented primarily by singly excited configurations, $^1\chi_{a\rightarrow r}$ and $^3\chi_{a\rightarrow r}$, where a and r are the occupied and virtual molecular orbitals (MOs) determined using the self-consistent-field (SCF) method for the ground state configuration, $^1\chi_0$. Hence, the expressions for the excitation energies are $E(^1\chi_{a\rightarrow r}) - E(^1\chi_0) = \varepsilon_r - \varepsilon_a - J_{ar} + 2K_{ar}$ and $E(^3\chi_{a\rightarrow r}) - E(^1\chi_0) = \varepsilon_r - \varepsilon_a - J_{ar}$, indicating $STG = E(^1\chi_{a\rightarrow r}) - E(^3\chi_{a\rightarrow r}) = 2K_{ar}$ (twice the exchange integral). As the overlap between the densities of the a and r MOs diminishes, a reduction in K_{ar} leads to degenerate S_1 and T_1 [8]. Along with vanishing K_{ar} , a decrease in the percentage contribution of the $^1\chi_{a\rightarrow r}$ configuration and an increased contribution from the doubly-excited configuration, $^1\chi_{aa\rightarrow rrr}$, was hypothesized to be a factor to selectively stabilize the S_1 state over T_1 resulting in a negative STG[9].

In 2019, two independent studies confirmed STGs < 0 in the prototypical cycl[3.3.3]azines—cyclazine[12] and

heptazine[13]—using time-dependent density functional theory (TDDFT) approximations, as well as a few correlated wavefunction methods. Since then, there has been a renewed interest in exploring the historically significant inverse-STG candidates: N-containing triangular molecules[14–22] and non-alternant hydrocarbons[23–25]. Besides these classes of molecules, Bedogni *et al.*[20] showed the possibility of $STG < 0$ in $C_nH_nN_n$ aza-rings.

Despite mounting computational evidence supporting the likelihood of Hund’s rule violation, the credibility of negative STGs still attracts criticisms[26]. This skepticism arises from the failure to account for the experimental conditions in computational modeling and the challenges posed by the large molecules for accurate *ab ini-*

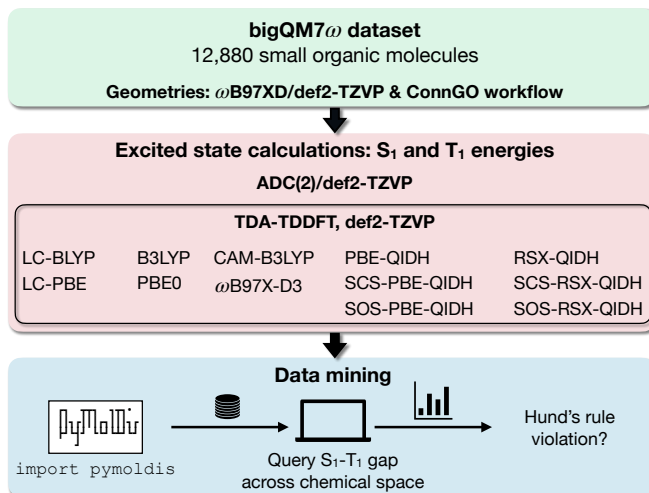


FIG. 1. Workflow outlining the design of the `pymoldis` module[10] for data mining S_1 and T_1 energies across 12,880 molecules with up to 7 CONF atoms in the bigQM7 ω dataset[11]. ADC(2) and TDDFT calculations were performed as a part of the present work. See Supplementary Information (SI) for screenshots of example queries.

* ramakrishnan@tifrh.res.in

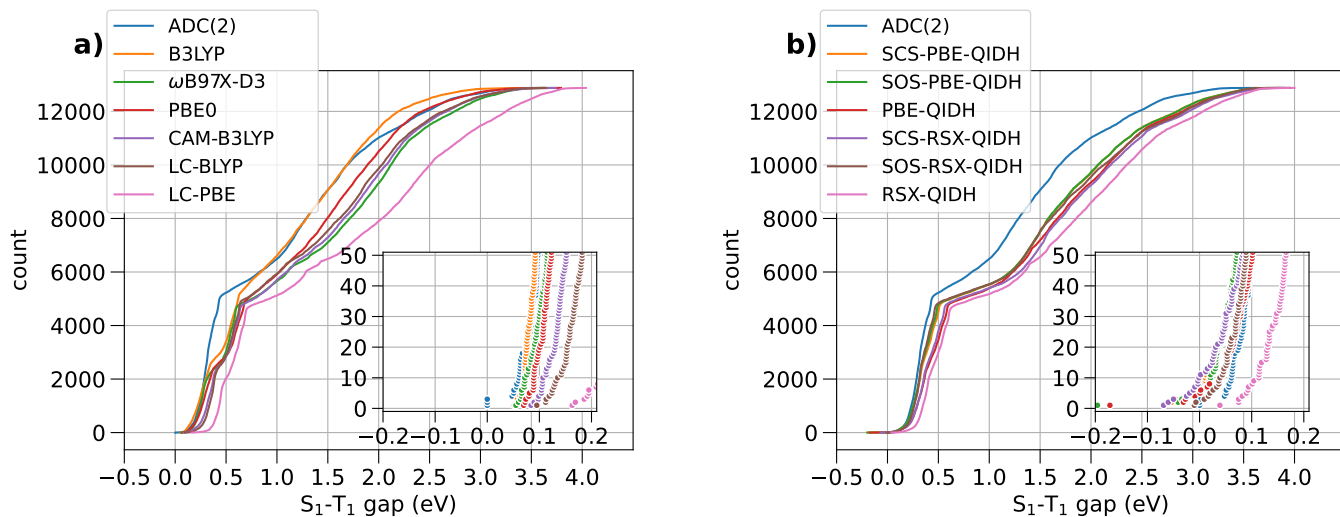


FIG. 2. Cumulative distribution of S_1 - T_1 energy gaps of 12,880 bigQM7 ω molecules calculated with various *ab initio* methods. The inset shows the distribution in the range of -0.2 to 0.2 eV.

tio calculations. More recently, Loos *et al.*[27] confirmed negative STGs in triangulene systems through composite excited states modeling and provided theoretical best estimates (TBEs).

The present study aims to report STGs calculated using a many-body method and double-hybrid density functional theory (dh-DFT) models for 12,880 small organic molecules with systematically varying compositions and structures. Using this data, we verify the possibility of Hund’s rule violation in the chemical space. Our workflow for data generation and the design of the module `pymoldis` for querying the reported data is illustrated in FIG. 1. The rest of this article discusses the qualitative aspects of the data, their analysis, and the technical details of the calculations.

II. RESULTS AND DISCUSSIONS

FIG. 2 shows the range spanned by the STGs of all the molecules in the bigQM7 ω dataset determined using various *ab initio* methods in the form of cumulative distributions. In both subplots (a and b) of this figure, ADC(2) is used as the reference theory for evaluating the accuracy of other methods. In the Supplementary Information (SI), we have discussed the accuracy of ADC(2) in combination with the def2-TZVP basis set for modeling STG of 10 triangle-shaped molecules using TBEs reported in a previous study[27]. Additionally, we have benchmarked the performance of the TDDFT version of SCS-PBE-QIDH within the Tamm–Dancoff approximation (TDA), see Tables S1–S4.

FIG. 2a shows the cumulative count of STG of 12,880 molecules predicted with ADC(2) and selected hybrid-, long-range-corrected-DFT, and long-range-corrected-hybrid-DFT approximations. All the theoretical mod-

els featured in this plot predict positive STGs. Past studies[19, 28, 29] have shown that explicit incorporation of electron correlation, for example, at the MP2-level (second-order many-body perturbation theory) as in dh-DFT, is a requirement to predict $STG < 0$. However, it has come as a surprise that at the ADC(2) level, which is the excited-state counterpart of MP2, none of the 12,880 molecules show a negative STG. Similar results from dh-DFT methods, along with their spin-component-scaled (SCS) and opposite-spin-component-scaled (SOS), are shown in FIG. 2b. The zoomed-in inset shows the distribution of values from RSX-QIDH to shift towards the positive domain compared to ADC(2) values. Upon SCS/SOS corrections[30], the distribution is shifted slightly to the negative domain. At the dh-DFT level, SCS-PBE-QIDH, an accurate method for modeling STGs of triangulenes, a few molecules exhibit $STG < 0$ eV; we give a detailed discussion of individual values later.

FIG. 3 illustrates the effect of SCS corrections to PBE-QIDH predicted values of STG in the form of probability densities of the shift in S_1 and T_1 energies with the inclusion of SCS. Overall, the SCS corrections lower the S_1 energy while raising the T_1 values, illustrating why SCS-PBE-QIDH favors smaller STG values than the unscaled method, PBE-QIDH. Figure S1 of the SI displays similar plots for SOS-PBE-QIDH, SCS-RSX-QIDH, and SOS-RSX-QIDH. While the SCS/SOS variants of RSX-QIDH shift the S_1 and T_1 energies further apart compared to the PBE-QIDH variants, previous benchmark studies[27, 31] have shown SCS-PBE-QIDH to be more accurate for modeling molecules with negative STGs. Hence, one can conclude that scaled-RSX-QIDH results in more false-positive predictions (*i.e.* spurious predictions of $STG < 0$ eV) than scaled-PBE-QIDH. Notably, the SCS/SOS corrections applied to the PBE-QIDH and

RSX-QIDH dh-DFT methods are specifically tailored for the TD-DFT framework[30]. Hence, STGs predicted using the Δ SCF approach will be similar in unscaled and scaled DFT methods.

The scatterplot in FIG. 4 offers a detailed view of the distribution of STG values around 0 eV. We find that the predominant entries shown in this plot are in the blue region denoted “True negatives in SCS-PBE-QIDH”, implying the TDDFT method agrees with ADC(2), both predicting these molecules as Hund’s rule obeying systems with positive STGs. Molecules shown in the red region of FIG. 4 are “False positives in SCS-PBE-QIDH” as these systems show $STG > 0.04$ eV according to ADC(2), while in the TDDFT formalism they show $STG < 0$ eV. As already highlighted in FIG. 2, there are no “True positives” or “False negatives” as none of the 12,880 molecules in the bigQM7 ω dataset exhibit a negative STG at the ADC(2) level.

The boundary separating positives and negatives in FIG. 4 is not sharp as both ADC(2) and SCS-PBE-QIDH have uncertainties > 0.1 eV in their predictions (see benchmarks in the SI). Figure S2 shows scatterplots of the joint distributions of STG with the S_1 and T_1 energies at both the SCS-PBE-QIDH and ADC(2) methods. At both levels of theories, one finds the small STG systems to have S_1 and T_1 energies in the range of 6–8 eV. Additionally, we find a molecule with S_1 and T_1 energy values in the 3-4 eV range to have a small STG at the SCS-PBE-QIDH level (see Figure S2 c and Figure S2 d). By querying the dataset using the `pymoldis` module (see Figures S3–S12), we found the corresponding molecule to be 2,6-dihydro-1H-pyridin-3-one (SMILES: O=C1CNCC=C1), which is cyclohexenone with an N atom at the δ -position.

To identify geometrical aspects common to the small STG molecules, we have queried the `pymoldis` database

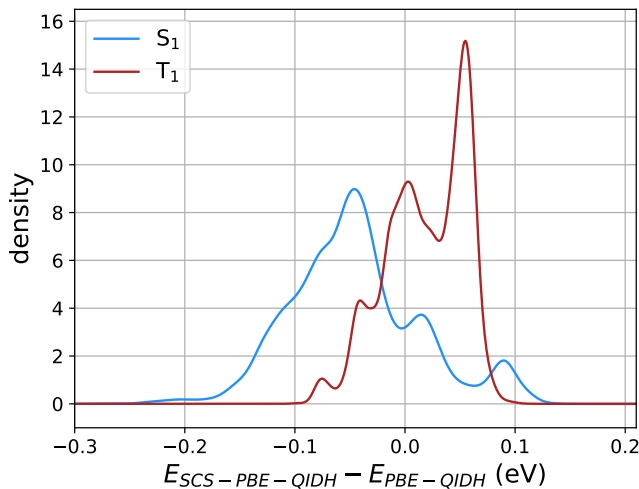


FIG. 3. Probability density of the shift in S_1 and T_1 energies (in eV) for 12,880 molecules upon the inclusion of spin-component-scaling (SCS) in PBE-QIDH.

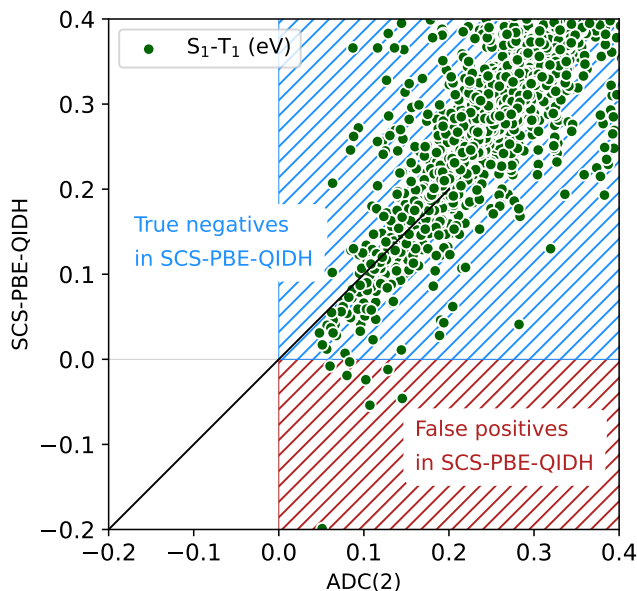


FIG. 4. Scatterplot of S_1 - T_1 energy gap ≤ 0.4 eV from SCS-PBE-QIDH and ADC(2) for the bigQM7 ω molecules.

for ten molecules with the smallest STG according to TDA/SCS-PBE-QIDH. FIG. 5 shows a screenshot of the query. A geometric moiety common to all N-containing systems is a substantial deviation of the bonding environment of the sp^3 -N center from the ideal geometry. While for the ten benchmark triangular systems, the S_1 and T_1 excitation energies are < 3 eV due to the possibility of a low-energy $n \rightarrow \pi^*$ transition, in the systems shown in FIG. 5, the S_1 / T_1 excitations are of the $n \rightarrow \sigma^*$ type with excitation energies > 6 eV. Nine of the ten molecules shown in FIG. 5 contain a 3-membered heterocyclic ring, while one is a fluorinated cyclopropane derivative; the S_1 and T_1 excitation energies of the latter are > 8 eV, at both TDDFT and ADC(2) levels while the corresponding $STG = -0.01$ eV and 0.13 eV at TDDFT and ADC(2) levels, respectively. The molecule corresponding to SMILES, CC1C2CCN1C2, in FIG. 5 contains a propellane-type cage with $STG = -0.01$ eV at the TDDFT level and an STG of 0.06 eV at the ADC(2) level. The bigQM7 ω dataset comprises several such cage systems with small STGs.

Starting with a cage-type molecule with a strained N, we have explored the possibility of designing a molecule with the character of the lowest excitation as $n \rightarrow \pi^*$. We started with a symmetric cage system, quinuclidine, a [2.2.2]propellane with an axial CH group replaced by an N atom, Structure 1 in FIG. 6. This molecule has an STG of 0.1 eV at the TDA-SCS-PBE-QIDH/def2-TZVP level. This small gap is because the excitation is primarily from non-bonding MO of N (highest occupied MO, HOMO) to C-H σ^* of the cage (lowest unoccupied MO, LUMO); their corresponding densities show poor overlap leading to a small value of exchange integral, K_{ar} .

```

import pymoldis
import pandas as pd

df=pymoldis.get_data('bigqm7w_S1T1')

S1T1_DFT=df['S1_SCSPEQIDH(eV)'] - df['T1_SCSPEQIDH(eV)']

NEntries=10

SmallGap_DFT_vals=S1T1_DFT.nsmallest(NEntries)

S1_DFT=df.iloc[SmallGap_DFT_vals.index]['S1_SCSPEQIDH(eV)']
T1_DFT=df.iloc[SmallGap_DFT_vals.index]['T1_SCSPEQIDH(eV)']
SMIs=df.iloc[SmallGap_DFT_vals.index]['SMI']

S1_ADC2=df.iloc[SmallGap_DFT_vals.index]['S1_ADC2(eV)']
T1_ADC2=df.iloc[SmallGap_DFT_vals.index]['T1_ADC2(eV)']
S1T1_ADC2=S1_ADC2-T1_ADC2

result = pd.concat([SMIs, S1_DFT, T1_DFT, SmallGap_DFT_vals, S1_ADC2, T1_ADC2, S1T1_ADC2], axis=1)
result.columns = ['SMI', 'DFT S1(eV)', 'DFT T1(eV)', 'DFT S1-T1(eV)', 'ADC2 S1(eV)', 'ADC2 T1(eV)', 'ADC2 S1-T1(eV)']

formatted_result = result.applymap(lambda x: f'{x:4.2f}' if isinstance(x, (int, float)) else x)

print(formatted_result.to_string(index=False))

```

SMI	DFT S1(eV)	DFT T1(eV)	DFT S1-T1(eV)	ADC2 S1(eV)	ADC2 T1(eV)	ADC2 S1-T1(eV)
'CC1(C)OC1(C)C'	8.08	8.28	-0.20	7.39	7.34	0.05
'CCC1(C)CN1C'	7.14	7.20	-0.05	6.73	6.62	0.11
'OC1CC2CN2C1'	7.31	7.36	-0.05	6.93	6.79	0.15
'CN1CC1(C)C'	7.14	7.16	-0.02	6.74	6.64	0.10
'CC1CCC2CN12'	7.42	7.44	-0.02	6.96	6.88	0.08
'CCC1(CF)CC1'	8.75	8.76	-0.01	8.56	8.44	0.13
'CC1C2CCN1C2'	7.21	7.22	-0.01	6.75	6.69	0.06
'CC1CCN2CC12'	7.41	7.41	-0.00	6.96	6.87	0.08
'CC1OC1(C)C'	8.48	8.47	0.01	7.64	7.56	0.08
'CN1CC1(C)CO'	7.32	7.31	0.01	6.97	6.82	0.14

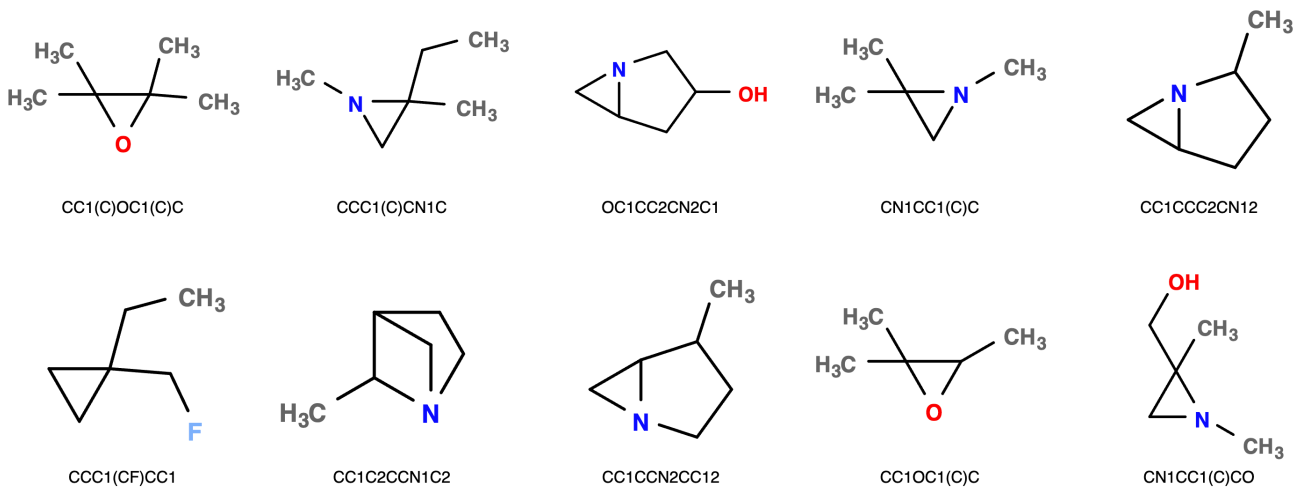


FIG. 5. Data-mining the bigQM7w dataset in pymoldis[10] to identify molecules with small S_1 - T_1 gaps. For the ten molecules with the lowest gaps according to TDA-SCS-PBE-QIDH, SMILES strings and S_1/T_1 energies are displayed. The corresponding ADC(2) values are also given alongside. Molecular structures are displayed in cartoon format below. See the SI for more examples of data-mining exercises.

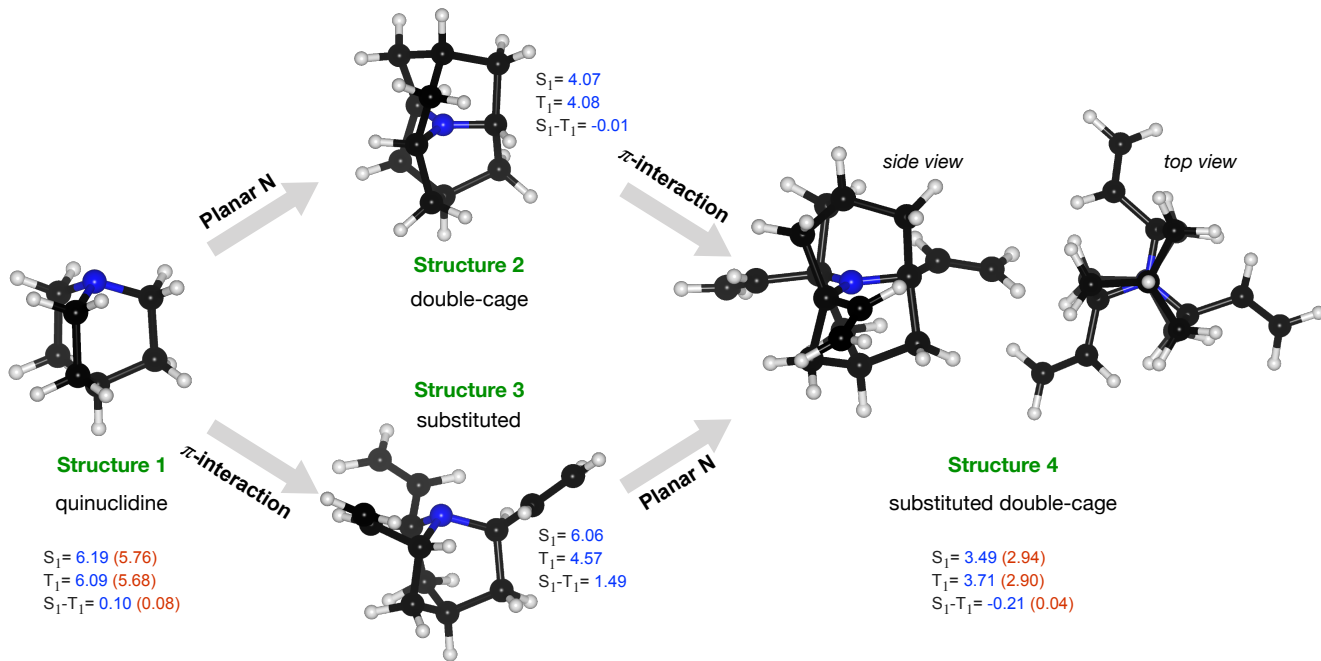


FIG. 6. TDA/SCS-PBE-QIDH predictions of S_1 , T_1 and $S_1 - T_1$ energies (in eV) of 1-azabicyclo[2.2.2]octane (aka quinuclidine) and its derivatives. For selected structures, additionally, ADC(2) values are in parentheses. White, black, and blue atoms correspond to H, C, and N atoms, respectively.

Further, to arrive at a local-geometric environment of the N atom as in cycl[3.3.3]azines, we have introduced an additional cage to constrain the N-center to a plane (Structure 2 in FIG. 6). This structure comprises perfectly co-planar C-N bonds resulting in degenerate $S_1 - T_1$ levels. We have also modified quinuclidine by attaching three ethylene groups (Structure 3). In this structure, the $S_0 \rightarrow S_1$ excitation has the character $n \rightarrow \pi^*$ (MO indices, $n:52$, which is the HOMO, and $\pi^*:53-55$) while the $S_0 \rightarrow T_1$ excitation has the character $\pi \rightarrow \pi^*$ (MO indices, $\pi:49-51$) with a large STG value of 1.5 eV. Finally, we combined structural modifications introduced in Structure 2 and Structure 3 to arrive at Structure 4 with a planar N interacting with π moieties through space. Interestingly, this system resulted in an STG of -0.21 eV. To verify this prediction of an inverse-STG nature, we have also performed ADC(2)/def2-TZVP calculations. For both Structure 1 and Structure 4, we find the magnitudes of the ADC(2) excitation energies to be lower than the DFT values. While both energies drop by a similar magnitude in the former, in Structure 4, the energy of T_1 drops more than the S_1 energy, giving rise to a nearly zero STG at the ADC(2) level. This case study indicates that for molecules such as Structure 4, even some of the best double-hybrid DFT methods can spuriously predict a negative STG; hence, one must consider many-body methods such as ADC(2) as a baseline theory.

While Structure 4 is a minimum on the potential energy surface as verified through vibrational frequency

analysis, we do not expect the system to be relevant to the thermally activated delayed fluorescence (TADF) applications[12, 15, 32–34]. On the other hand, it is a compelling computational chemistry exercise to modulate a molecule’s STG by chemical modifications. Hence, even though Structure 4 seems to be yet another false positive in the search for a Hund’s rule-violating molecule, we have examined it further. We inspected the shape of the MOs involved in the S_1 and T_1 excitations and found the excitations to be primarily HOMO \rightarrow LUMO type. These MOs are on display in FIG. 7, from which we visually conclude that the densities of HOMOs and LUMOs do not overlap. For a more quantitative analysis, we calculated the Λ -index[35] defined as $\int d\mathbf{r} |\phi_a(\mathbf{r})| |\phi_r(\mathbf{r})|$ using Multiwfn[36], and obtained the values: 0.37 and 0.40 for the S_1 and the T_1 states, respectively. The Λ -index quantifies the degree of overlap between hole and electron in $S_0 \rightarrow S_1$ and $S_0 \rightarrow T_1$ excitations. In comparison, for cyclazine and heptazine, the values of Λ for the S_1/T_1 states are 0.49/0.49 and 0.50/0.51, respectively.

III. COMPUTATIONAL DETAILS

The bigQM7 ω dataset [11, 37] features 12,880 molecules with up to 7 CONF atoms with equilibrium geometries determined with the ω B97X-D DFT method and the def2-TZVP basis set. Molecular graphs of bigQM7 ω molecules, encoded as SMILES, were sourced

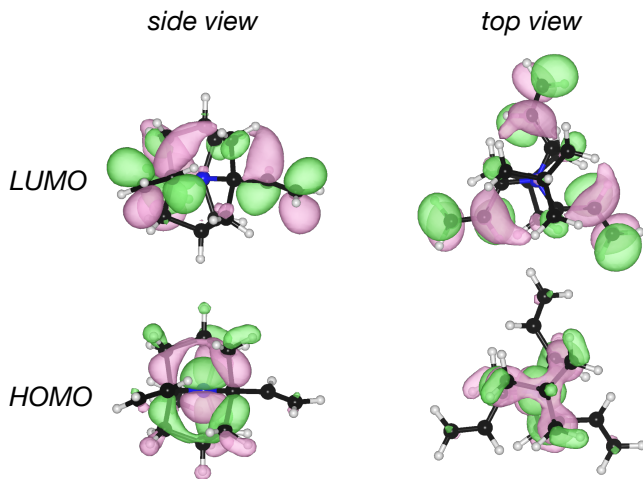


FIG. 7. Plots of HOMO and LUMO of the ethylene substituted double cage derivative of quinuclidine, Structure 4, shown in FIG. 6.

from the GDB11[38] chemical space, which contains several common molecules, such as acetic acid and benzoic acid, which the subsequent databases GDB13[39] and GDB17[40] filtered out. Consequently, bigQM7 ω offers over thrice the number of molecules with up to 7 CONF atoms than the QM9 dataset[41] derived from GDB17. The geometries of the bigQM7 ω molecules were optimized[11] using the connectivity preserving geometry optimization (ConnGO) workflow to prevent covalent bond rearrangements during geometry optimization[42]. Further, vibrational frequency analysis at the ω B97X-D/def2-TZVP level verified each structure in bigQM7 ω to be an energy minimum. Along with the minimum energy geometries, bigQM7 ω offers several ground-state properties ranging from partial charges to thermochemistry energies along with excited state properties[37].

For all 12,880 molecules in bigQM7 ω , we performed single-point vertical excited state calculations of the S_1 and T_1 energies using 12 DFT methods: PBE0 [43], B3LYP [44], CAM-B3LYP [45], ω B97X-D3[46], LC-BLYP [47], LC-PBE [48], PBE-QIDH [49], SCS-PBE-QIDH, SOS-PBE-QIDH[30], RSX-QIDH[50], SCS-RSX-QIDH [30] and SOS-RSX-QIDH [30]. We also calculated S_1 and T_1 energies using the correlated excited state method: second-order algebraic diagrammatic construction, ADC(2). The accuracy of ADC(2) and SCS-PBE-QIDH in combination with other settings is evaluated in the SI using previously reported[27] TBES of 10 triangular systems as references. For this purpose, we performed geometry optimization of the triangular molecules using the ω B97X-D3 DFT method with `tightscf` and `tightopt` keywords in combination with the def2-TZVP basis set. Minimum energy structures and S_1/T_1 energies of the bigQM7 ω can be queried using the `pymoldis` module presented in this study (See Figure S08 and Figure S12 in the SI).

We performed ADC(2) calculations using QChem 6.0.2

and DFT calculations using ORCA 5.0.4[51, 52]. With in TDDFT, we calculated twelve energy eigenvalues—six singlets and six triplets—which we sorted separately to extract S_1 and T_1 (lowest excited triplet) TDDFT excitation energies. In all calculations, we used the resolution-of-identity (RI) approximation[53, 54]. In DFT calculations, we used the ‘chain-of-spheres’ (COS) algorithm for exchange integrals (RIJCOSX). In dh-DFT calculations, we used the universal fitting auxiliary basis sets by Weigend [55] (denoted def2/J) along with the def2-TZVP/C and aug-cc-pVTZ/C basis sets for the orbital basis sets def2-TZVP, and aug-cc-pVTZ, respectively.

IV. CONCLUSIONS

We have probed the violation of Hund’s rule in the chemical space of about 13,000 small organic molecules with up to 7 atoms of C/O/N/F. We performed high-throughput calculations of excited states with various DFT methods and the more accurate theory ADC(2). We selected these methods based on their accuracy in benchmark calculations and compared them with previously reported theoretical best estimates for the STGs of ten triangular molecules. ADC(2) with a triple-zeta basis set provides an effective cost-accuracy trade-off for generating large-scale data. Further, this method has been shown[27] to agree with composite excited state methods for predicting $STG < 0$ with an average error of < 0.05 eV. The critical result of the present study is that Hund’s rule[56] prevails across thousands of organic molecules with systematically varying structures covering almost all prototypical small organic molecules.

The data presented in this study is importable in Python code for data mining endeavors. Using this infrastructure, we identified molecules with vanishing STG, some of which have negative values at the SCS-PBE-QIDH level while not violating Hund’s rule as per ADC(2) predictions. A common geometric feature of these molecules was a substantial deviation of an N-atom from the typical sp^3 environment with both singlet and triplet excitations showing the $n \rightarrow \sigma^*$ character and potentially vanishing exchange interaction integral between the MOs involved in excitation.

We have selected a cage structure and attached ethylene groups to mimic the environment of the N atom as in the well-known cases of cycl[3.3.3]azines. The corresponding MOs involved in S_1/T_1 excitations exhibit characteristics seen in previously studied triangular negative-STG systems. Upon further scrutiny, we showed this molecule as a conventional molecule obeying Hund’s rule. Yet, introducing a polarizable environment in this system through donor-acceptor groups may selectively stabilize the S_1 over T_1 [12, 25]. In this study, we did not investigate the practical utility of the small molecules studied in the context of TADF. Such exploration necessitates meticulous consideration of adiabatic effects on a case-by-case basis, a task that exceeds the scope of our present

investigation. The present study demonstrates that a data-driven approach allows for gaining insight into the molecular structural factors that can quench the singlet-triplet energy gap. We offered evidence that the chemical space of small closed-shell organic molecules lack geometric and electronic structural necessary for a negative S_1 - T_1 energy gap.

Theoretical studies have identified only a few molecular fingerprints to favor negative STGs. Dynamic spin polarization, attributed to double excitation effects involving frontier orbitals, has emerged as a potential mechanism to induce a negative STG [1, 57, 58]. While a quantitative relationship exists between molecular structural features and zero STG, a corresponding structure-property relation for negative STG remains elusive. Introducing functional groups is one promising avenue for designing large synthetically tractable molecules with negative STG. For theoretical explorations, our research highlights the limitations of using DFT methods, which can result in false positives. Consequently, there is a pressing need for efficient strategies to accelerate predictions using correlated wavefunction methods. For large-scale investigations, data-driven modeling can complement first-principles modeling combined with inverse-design strategies, such as those based on genetic algorithms[59, 60].

V. SUPPLEMENTARY INFORMATION

Contains the following: Assessment of S_1 - T_1 gaps from ADC(2) and SCS-PBE-QIDH for 10 triangular molecules. Table S1 compares S_1/T_1 energetics calculated using the ADC(2) method with theoretical best estimates. Table S2 compares the S_1/T_1 energetics predicted by TDDFT and TDA. Table S3 contains ADC(2) and TDA energies calculated using DFT-level geometries. Table S4 provides various error metrics for ADC(2) and SCS-PBE-QIDH predicted S_1/T_1 energetics. Figure S1 illustrates the shifts in S_1 and T_1 due to SCS/SOS corrections to PBE-QIDH and RSX-QIDH methods. Figure S2 shows a scatterplot of S_1 and T_1 energies with S_1 - T_1 gaps. Figures S3–S12 offer screen-

shots of data mining exercises. Minimum energy geometries of Structures 1–4 in FIG. 6 are also listed. Sample Python notebooks and further details are available at <https://github.com/moldis-group/pymoldis>[10].

VI. DATA AVAILABILITY

The data that support the findings of this study are within the article and its supplementary material.

VII. ACKNOWLEDGMENTS

We acknowledge the support of the Department of Atomic Energy, Government of India, under Project Identification No. RTI 4007. All calculations have been performed using the Helios computer cluster, which is an integral part of the MolDis Big Data facility, TIFR Hyderabad (<http://moldis.tifrh.res.in>).

VIII. AUTHOR DECLARATIONS

A. Author contributions

AM: Conceptualization (equal); Analysis (equal); Data collection (equal); Writing (equal); Revision (equal). **RR:** Conceptualization (equal); Analysis (equal); Data collection (equal); Funding acquisition; Project administration and supervision; Resources; Writing (equal); Revision (equal).

B. Conflicts of Interest

The authors have no conflicts of interest to disclose.

REFERENCES

-
- [1] H. Kollmar and V. Staemmler, *Theor. Chim. Acta* **48**, 223 (1978).
- [2] S. Koseki, T. Nakajima, and A. Toyota, *Can. J. Chem.* **63**, 1572 (1985).
- [3] W. T. Borden, H. Iwamura, and J. A. Berson, *Acc. Chem. Res.* **27**, 109 (1994).
- [4] A. Toyota and T. Nakajima, *J. Chem. Soc., Perkin trans.*, 1731 (1986).
- [5] A. Toyota, *Theor. Chim. Acta* **74**, 209 (1988).
- [6] D. A. Hrovat and W. T. Borden, *J. Mol. Struct. (THEOCHEM)* **398**, 211 (1997).
- [7] J. C. Sancho-Garcia, E. Bremond, G. Ricci, A. Pérez-Jiménez, Y. Olivier, and C. Adamo, *J. Chem. Phys.* **156** (2022).
- [8] W. Leupin and J. Wirz, *J. Am. Chem. Soc.* **102**, 6068 (1980).
- [9] V. Bonacic-Koutecky and J. Michl, *J. Am. Chem. Soc.* **107**, 1765 (1985).
- [10] R. Ramakrishnan, “pymoldis: A python suite for molecular discovery using quantum chemistry big data,” (2021).
- [11] P. Kayastha, S. Chakraborty, and R. Ramakrishnan, *Digital Discov.* **1**, 689 (2022).
- [12] P. de Silva, *J. Phys. Chem. Lett.* **10**, 5674 (2019).
- [13] J. Ehrmaier, E. J. Rabe, S. R. Pristash, K. L. Corp, C. W. Schlenker, A. L. Sobolewski, and W. Domcke, *J. Phys. Chem. A* **123**, 8099 (2019).

- [14] J. Sanz-Rodrigo, G. Ricci, Y. Olivier, and J.-C. Sancho-García, *J. Phys. Chem. A* **125**, 513 (2021).
- [15] R. Pollice, P. Friederich, C. Lavigne, G. dos Passos Gomes, and A. Aspuru-Guzik, *Matter* **4**, 1654 (2021).
- [16] G. Ricci, E. San-Fabián, Y. Olivier, and J.-C. Sancho-García, *ChemPhysChem* **22**, 553 (2021).
- [17] A. L. Sobolewski and W. Domcke, *J. Phys. Chem. Lett.* **12**, 6852 (2021).
- [18] N. Aizawa, Y.-J. Pu, Y. Harabuchi, A. Nihonyanagi, R. Ibuka, H. Inuzuka, B. Dhara, Y. Koyama, K.-i. Nakayama, S. Maeda, *et al.*, *Nat. Commun* **609**, 502 (2022).
- [19] L. Tučková, M. Straka, R. R. Valiev, and D. Sundholm, *Phys. Chem. Chem. Phys* **24**, 18713 (2022).
- [20] M. Bedogni, D. Giavazzi, F. Di Maiolo, and A. Painelli, *J. Chem. Theory Comput.* (2023).
- [21] H. Kim, G. Scholes, and S. K. Min, *Phys. Chem. Chem. Phys.* (2024).
- [22] D. Blasco, R. Nasibullin, R. R. Valiev, M. Monge, J. M. López-de Luzuriaga, and D. Sundholm, *Phys. Chem. Chem. Phys.* (2024).
- [23] J. Terence Blaskovits, M. H. Garner, and C. Corminboeuf, *Angew. Chem. Int. Ed.* **62**, e202218156 (2023).
- [24] M. E. Sandoval-Salinas, G. Ricci, A. Pérez-Jiménez, D. Casanova, Y. Olivier, and J.-C. Sancho-García, *Phys. Chem. Chem. Phys.* **25**, 26417 (2023).
- [25] M. H. Garner, J. T. Blaskovits, and C. Corminboeuf, *Chem. Commun.* (2024).
- [26] A. Dreuw and M. Hoffmann, *Front. Chem.* **11** (2023).
- [27] P.-F. Loos, F. Lipparini, and D. Jacquemin, *J. Phys. Chem. Lett.* **14**, 11069 (2023).
- [28] S. Ghosh and K. Bhattacharyya, *J. Phys. Chem. A* **126**, 1378 (2022).
- [29] M. Kondo, *Chem. Phys. Lett.* **804**, 139895 (2022).
- [30] M. C. Paez and L. Goerigk, (2021).
- [31] M. Alipour and T. Izadkhast, *J. Chem. Phys.* **156** (2022).
- [32] J. Li, Z. Li, H. Liu, H. Gong, J. Zhang, Y. Yao, and Q. Guo, *Front. Chem.* **10**, 999856 (2022).
- [33] X. Wang, A. Wang, M. Zhao, and N. Marom, *J. Phys. Chem. Lett.* **14**, 10910 (2023).
- [34] T. Won, K.-i. Nakayama, and N. Aizawa, *Chem. Phys. Rev.* **4** (2023).
- [35] M. J. Peach, P. Benfield, T. Helgaker, and D. J. Tozer, *J. Chem. Phys.* **128** (2008).
- [36] T. Lu and F. Chen, *J. Comput. Chem.* **33**, 580 (2012).
- [37] P. Kayastha and R. Ramakrishnan, “bigQM7 ω : A high-quality dataset of ground-state properties and excited state spectra of 12880 molecules containing up to 7 atoms of CONF,” (2021).
- [38] T. Fink, H. Bruggesser, and J.-L. Reymond, *Angew. Chem. Int. Ed.* **44**, 1504 (2005).
- [39] L. C. Blum and J.-L. Reymond, *J. Am. Chem. Soc.* **131**, 8732 (2009).
- [40] L. Ruddigkeit, R. Van Deursen, L. C. Blum, and J.-L. Reymond, *J. Chem. Inf. Model.* **52**, 2864 (2012).
- [41] R. Ramakrishnan, P. O. Dral, M. Rupp, and O. A. Von Lilienfeld, *Sci. data* **1**, 1 (2014).
- [42] S. Senthil, S. Chakraborty, and R. Ramakrishnan, *Chem. Sci.* **12**, 5566 (2021).
- [43] C. Adamo and V. Barone, *J. Chem. Phys.* **110**, 6158 (1999).
- [44] P. J. Stephens, F. J. Devlin, C. F. Chabalowski, and M. J. Frisch, *J. Chem. Phys.* **98**, 11623 (1994).
- [45] T. Yanai, D. P. Tew, and N. C. Handy, *J. Phys. Chem. Lett.* **393**, 51 (2004).
- [46] J.-D. Chai and M. Head-Gordon, *Phys. Chem. Chem. Phys.* **10**, 6615 (2008).
- [47] Y. Tawada, T. Tsuneda, S. Yanagisawa, T. Yanai, and K. Hirao, *J. Chem. Phys.* **120**, 8425 (2004).
- [48] H. Iikura, T. Tsuneda, T. Yanai, and K. Hirao, *J. Chem. Phys.* **115**, 3540 (2001).
- [49] É. Brémond, J. C. Sancho-García, Á. J. Pérez-Jiménez, and C. Adamo, *J. Chem. Phys.* **141** (2014).
- [50] E. Bremond, M. Savarese, Á. J. Pérez-Jiménez, J. C. Sancho-García, and C. Adamo, *J. Chem. Theory Comput.* **14**, 4052 (2018).
- [51] F. Neese, *Wiley Interdiscip. Rev. Comput. Mol. Sci.* **2**, 73 (2012).
- [52] F. Neese, *Wiley Interdiscip. Rev. Comput. Mol. Sci.* **8**, e1327 (2018).
- [53] O. Vahtras, J. Almlöf, and M. Feyereisen, *Chem. Phys. Lett.* **213**, 514 (1993).
- [54] R. A. Kendall and H. A. Früchtel, *Theor. Chim. Acta* **97**, 158 (1997).
- [55] F. Weigend, *Phys. Chem. Chem. Phys.* **8**, 1057 (2006).
- [56] W. Kutzelnigg and J. Morgan, *Z. Phys. D - Atoms Molec. Clusters* **36**, 197 (1996).
- [57] R. Pollice, B. Ding, and A. Aspuru-Guzik, *Matter* **7**, 1161 (2024).
- [58] D. Drwal, M. Matousek, P. Golub, A. Tucholska, M. Hapka, J. Brabec, L. Veis, and K. Pernal, *J. Chem. Theory Comput.* **19**, 7606 (2023).
- [59] A. Nigam, R. Pollice, P. Friederich, and A. Aspuru-Guzik, *Chem. Sci.* (2024).
- [60] A. Gupta, S. Chakraborty, D. Ghosh, and R. Ramakrishnan, *J. Chem. Phys.* **155** (2021).

Supplementary information for:

Resilience of Hund’s rule in the Chemical Space of Small Organic Molecules

Atreyee Majumdar and Raghunathan Ramakrishnan*

Tata Institute of Fundamental Research Hyderabad, Hyderabad 500046, India.

E-mail: ramakrishnan@tifrh.res.in

Assessment of methods for data-generation

For calculating the energies of the S_1 and T_1 excited states of all molecules in the bigQM7 ω dataset, we have evaluated the cost-accuracy trade-off in various approximations stemming from the choice of the basis set, accuracy of geometries, approximation of molecular integrals with resolution-of-identity, and the Tamm-Dancoff approximation (TDA) to time-dependent density functional theory (TDDFT). To this end, we have selected ten triangular molecules from a previous study¹ with the theoretical best estimates (TBEs) for the energies of S_1 and T_1 determined using frozen-core CCSD(T)/cc-pVTZ geometries. From the same study, we collected energies from ADC(2) and the TDDFT-SCS-PBE-QIDH methods using the aug-cc-pVTZ basis set. With these values as references, we evaluated the accuracy of ADC(2) and TDA using the smaller basis set def2-TZVP.

For all benchmark systems, S_1 and T_1 energies, along with the S_1 - T_1 gaps determined with various theoretical methods, are collected in Table S1, Table S2, and Table S3. The accuracies of different methods are quantified via the error metrics, mean signed error (MSE), mean absolute error (MAE), standard deviation of the error (SDE), minimum error (minE),

and maximum error (maxE) in Table S4. We evaluate these metrics using the aforesaid TBEs¹ as the reference. To understand the impact of the choice of geometries, we have performed geometry optimization of these ten molecules at the ω B97X-D3/def2-TZVP level.

From Table S1, we find that when using frozen-core CCSD(T)/cc-pVTZ geometries, ADC(2)/def2-TZVP predicts similar energies as ADC(2)/aug-cc-pVTZ. However, the error metrics in Table S4 suggest that for all S_1 - T_1 gaps, the SDE drops from 0.034 eV to 0.011 eV, indicating the smaller basis set def2-TZVP to perform better in the ADC(2) calculations. We also note similar improvement for S_1 and T_1 energies. This trend is in line with the observation made in an earlier study² that ADC2/aug-cc-pVDZ yields a more accurate S_1 - T_1 gap for triangular molecules than ADC(2)/aug-cc-pVTZ due to a favorable error cancellation. ADC(2)/def2-TZVP values determined using ω B97X-D3/def2-TZVP geometries (see Table S3) very closely resemble ADC(2)/def2-TZVP values determined using CCSD(T)/cc-pVTZ geometries (see Table S1). Further, while the change in geometry has a small influence on the error metrics for S_1 and T_1 energies, due to the cancellation of effects, the metrics for the S_1 - T_1 gap are less influenced.

We also compare the TDDFT/SCS-PBE-QIDH/aug-cc-pVTZ (determined using CCSD(T)/cc-pVTZ geometries) results from Ref. 1, to TDA analog in Table S2. In this Table, we have also reported TDDFT values calculated by us using geometries from Ref. 1 and find our results to agree with previously reported values precisely, assuring that our computational settings are consistent with the previous study. Moving from TDDFT to TDA, the largest effect is seen for molecule 6. At the TDDFT level, this system’s S_1 - T_1 gap is -0.32 eV, which increases to -0.03 eV at the TDA level. However, we find the TDA value better to approximate the TBE value of -0.07 eV from Table S1. For the S_1 - T_1 gap, TDDFT values of MSE, MAE, and SDE are -0.033 , 0.055 , and 0.081 eV, respectively, which drop to 0.034 , 0.034 , and 0.012 eV when using TDA. The SDE of TDA is 8-fold smaller than that of TDDFT, indicating smaller non-systematic errors in the predictions.

The TDA calculations when performed using def2-TZVP basis set, in combinaton with

ω B97X-D3/def2-TZVP geometries (Table S3), result in increasing MSE and MAE for S_1 and T_1 energies. However, due to the cancellation of effects, the MAE and SDE for the S_1 - T_1 gap are smaller than TDDFT/aug-cc-pVTZ and TDA/aug-cc-pVTZ (see Table S4); the latter two using CCSD(T)/cc-pVTZ geometries from Ref. 1.

Hence, combining the favorable effects of TDA and a smaller basis set, we have used TDA-TDDFT/def2-TZVP in combination with various DFT approximations to generate the excited state energetics of the bigQM7 ω dataset.

Table S1: Energies of the S_1 and T_1 states with respect to the S_0 ground state along with the singlet-triplet gap, S_1 - T_1 , of 10 triangular benchmark systems reported in Ref. 1. ADC(2)/def2-TZVP results are compared with theoretical best estimate (TBE) and ADC(2)/aug-cc-pVTZ values from Ref. 1. All values are in eV and # indicates compound number. In all calculations, we used geometries determined with the CCSD(T)/cc-pVTZ method reported in Ref. 1.

#	TBE ^a			ADC(2)/aug-cc-pVTZ ^a			ADC(2)/def2-TZVP ^b		
	S_1	T_1	S_1 - T_1	S_1	T_1	S_1 - T_1	S_1	T_1	S_1 - T_1
1	2.717	2.936	-0.219	2.675	2.921	-0.246	2.665	2.915	-0.250
2	0.979	1.111	-0.131	1.001	1.138	-0.137	1.001	1.139	-0.138
3	1.562	1.663	-0.101	1.551	1.664	-0.113	1.548	1.665	-0.117
4	2.177	2.296	-0.119	2.159	2.298	-0.139	2.153	2.295	-0.142
5	2.127	2.230	-0.103	2.098	2.225	-0.127	2.093	2.225	-0.132
6	0.833	0.904	-0.071	0.851	0.945	-0.094	0.854	0.950	-0.096
7	0.693	0.735	-0.042	0.708	0.782	-0.074	0.714	0.791	-0.078
8	0.554	0.583	-0.029	0.565	0.635	-0.070	0.575	0.646	-0.071
9	1.264	1.463	-0.199	1.274	1.488	-0.214	1.271	1.487	-0.216
10	1.522	1.827	-0.305	1.639	2.074	-0.435	1.526	1.840	-0.314

^a From Ref. 1.

^b This work.

Table S2: Energies of the S_1 and T_1 states with respect to the S_0 ground state along with the singlet-triplet gap, S_1-T_1 , of 10 triangular benchmark systems reported in Ref. 1. All energies were determined using TDDFT or its Tamm–Dancoff approximation (TDA) employing the SCS-PBE-QIDH double-hybrid DFT method and the aug-cc-pVTZ basis set. All values are in eV and # indicates compound number. In all calculations, we used geometries determined with the CCSD(T)/cc-pVTZ method reported in Ref. 1.

#	TDDFT/aug-cc-pVTZ ^a			TDDFT/aug-cc-pVTZ ^b			TDA/aug-cc-pVTZ ^b		
	S_1	T_1	S_1-T_1	S_1	T_1	S_1-T_1	S_1	T_1	S_1-T_1
1	2.770	2.987	-0.217	2.770	2.986	-0.216	2.845	3.055	-0.210
2	1.039	1.163	-0.124	1.037	1.161	-0.124	1.112	1.196	-0.084
3	1.621	1.685	-0.064	1.620	1.685	-0.065	1.696	1.749	-0.053
4	2.239	2.340	-0.101	2.238	2.339	-0.101	2.317	2.405	-0.088
5	2.188	2.245	-0.057	2.186	2.243	-0.057	2.264	2.331	-0.067
6	0.881	1.201	-0.320	0.879	1.202	-0.323	0.959	0.986	-0.027
7	0.728	0.825	-0.097	0.726	0.824	-0.098	0.809	0.808	0.001
8	0.574	0.673	-0.099	0.573	0.672	-0.099	0.658	0.647	0.011
9	1.305	1.538	-0.233	1.305	1.538	-0.233	1.398	1.567	-0.169
10	1.566	1.906	-0.340	1.566	1.906	-0.340	1.659	1.947	-0.288

^a From Ref. 1.

^b This work.

Table S3: ADC(2) and TDA-SCS-PBE-QIDH energies of the S_1 and T_1 states with respect to the S_0 ground state along with the singlet-triplet gap, S_1-T_1 , of 10 triangular benchmark systems reported in Ref. 1. All values are in eV and # indicates compound number. All calculations were performed using the def2-TZVP basis set, and geometries calculated with the ω B97X-D3/def2-TZVP method.

#	ADC(2)/def2-TZVP			TDA/def2-TZVP		
	S_1	T_1	S_1-T_1	S_1	T_1	S_1-T_1
1	2.691	2.935	-0.244	2.865	3.070	-0.205
2	1.021	1.158	-0.137	1.135	1.219	-0.084
3	1.569	1.684	-0.115	1.716	1.770	-0.054
4	2.175	2.313	-0.139	2.336	2.420	-0.084
5	2.115	2.243	-0.128	2.283	2.350	-0.067
6	0.884	0.982	-0.098	0.995	1.027	-0.032
7	0.752	0.830	-0.078	0.857	0.860	-0.003
8	0.620	0.689	-0.069	0.715	0.706	0.009
9	1.265	1.480	-0.215	1.390	1.558	-0.168
10	1.518	1.828	-0.310	1.648	1.931	-0.283

Table S4: Error metrics for predicting the S_1 & T_1 energetics of 10 triangular benchmark systems reported in Ref. 1. Values are reported for various theoretical methods in comparison with the theoretical best estimates from Ref. 1. MSE: mean signed error, MAE: mean absolute error, SDE: standard deviation of the error, minE: minimal error, maxE: maximal error are in eV.

Method	Energy	MSE	MAE	SDE	minE	maxE
ADC(2)/aug-cc-pVTZ ^a	S_1	0.009	0.029	0.041	-0.042	0.117
	T_1	0.042	0.046	0.072	-0.015	0.247
	S_1-T_1	-0.033	0.033	0.034	-0.130	-0.006
	mean	0.006	0.036	0.049	-0.062	0.119
ADC(2)/def2-TZVP ^b	S_1	-0.003	0.022	0.025	-0.052	0.022
	T_1	0.021	0.026	0.027	-0.021	0.063
	S_1-T_1	-0.024	0.024	0.011	-0.042	-0.007
	mean	-0.002	0.024	0.021	-0.038	0.026
ADC(2)/def2-TZVP ^c	S_1	0.018	0.027	0.031	-0.026	0.066
	T_1	0.040	0.040	0.038	-0.001	0.106
	S_1-T_1	-0.021	0.021	0.011	-0.040	-0.005
	mean	0.012	0.029	0.027	-0.022	0.056
TDDFT-SCS-PBE-QIDH/aug-cc-pVTZ ^a	S_1	0.048	0.048	0.013	0.020	0.062
	T_1	0.082	0.082	0.076	0.015	0.297
	S_1-T_1	-0.033	0.055	0.081	-0.249	0.046
	mean	0.032	0.062	0.057	-0.071	0.135
TDA-SCS-PBE-QIDH/aug-cc-pVTZ ^b	S_1	0.129	0.129	0.011	0.104	0.140
	T_1	0.094	0.094	0.018	0.064	0.120
	S_1-T_1	0.034	0.034	0.012	0.009	0.048
	mean	0.086	0.086	0.014	0.059	0.103
TDA-SCS-PBE-QIDH/def2-TZVP ^c	S_1	0.151	0.151	0.013	0.126	0.164
	T_1	0.116	0.116	0.011	0.095	0.134
	S_1-T_1	0.035	0.035	0.010	0.014	0.047
	mean	0.101	0.101	0.011	0.078	0.115

^a Using CCSD(T)/cc-pVTZ geometries from Ref. 1.

^b This work, using CCSD(T)/cc-pVTZ geometries from Ref. 1.

^c Using ω B97X-D3/def2-TZVP geometries, this work.

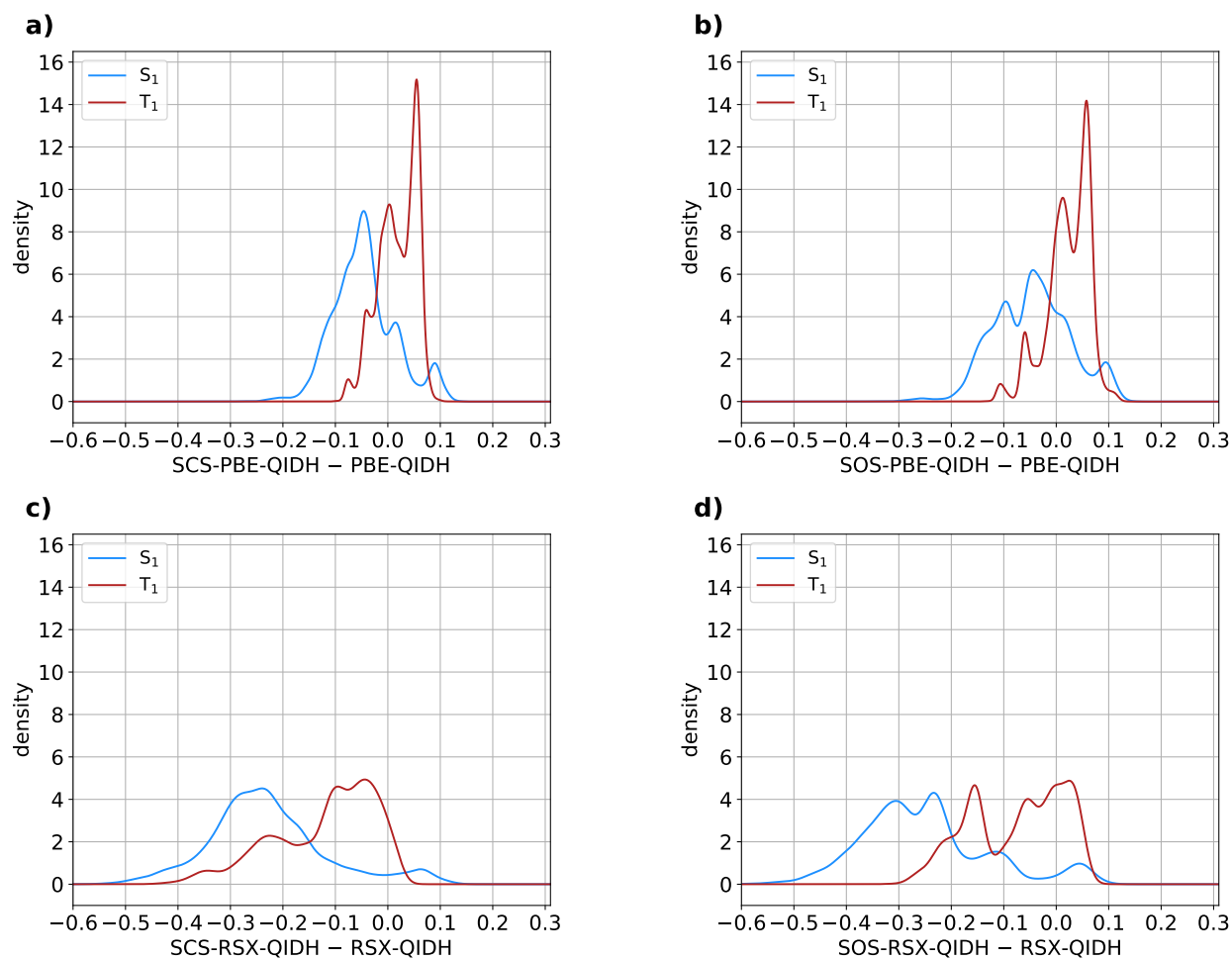


Figure S1: Probability density of the shift in S_1 and T_1 energies (in eV) of 12,880 molecules with the introduction of spin-component-scaling (SCS) and opposite-spin-component-scaling (SOS) in PBE-QIDH and RSX-QIDH methods.

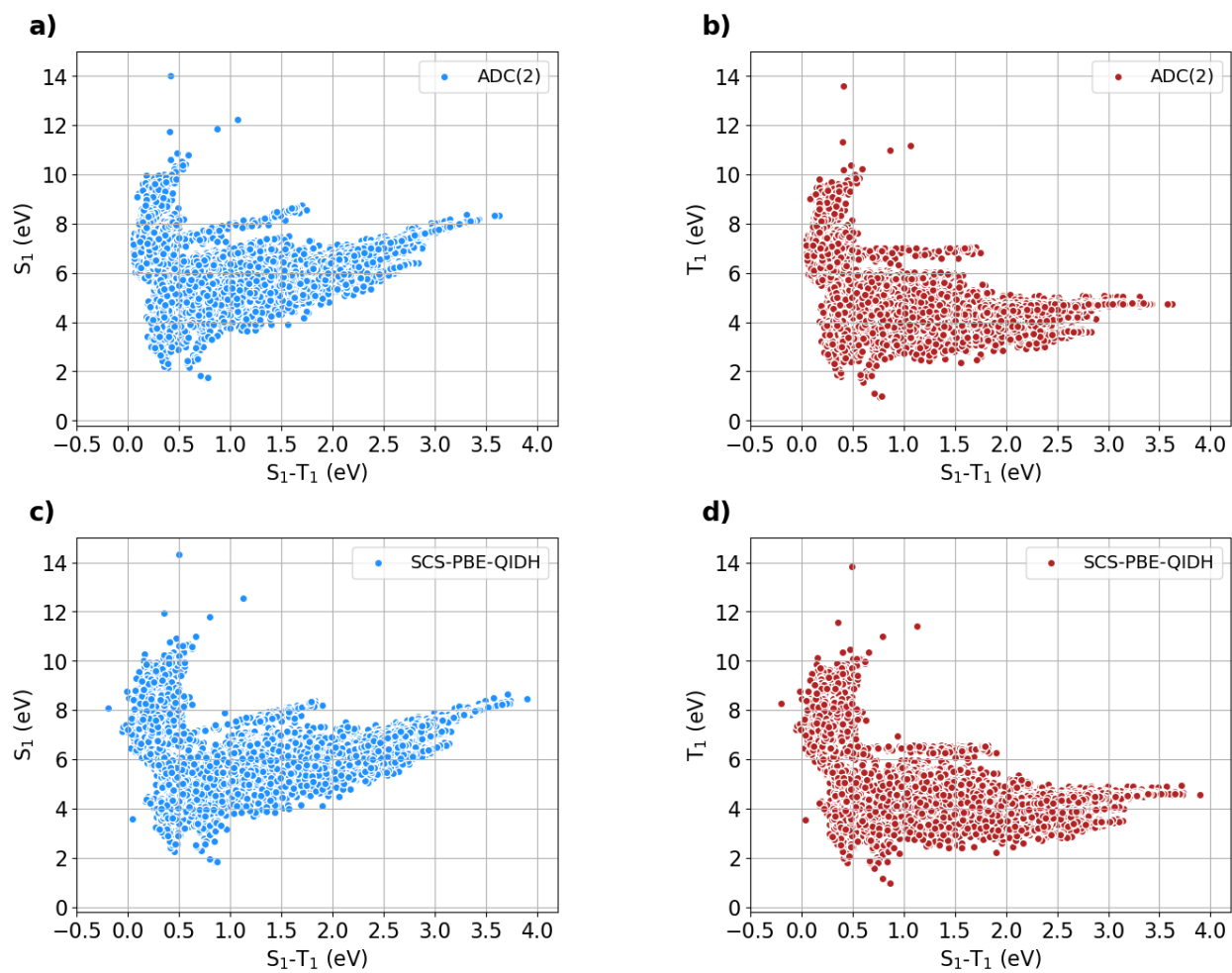


Figure S2: Distribution of S_1 and T_1 energies of 12,880 molecules calculated with ADC(2) and SCS-PBE-QIDH methods shown jointly with the $S_1 - T_1$ gap.

```
[1]: import pymoldis

df=pymoldis.get_data('bigqm7w_S1T1')
df.describe()
```

	Natoms	S1_SCSPEQIDH(eV)	T1_SCSPEQIDH(eV)	f01_SCSPEQIDH(au)	S1_ADC2(eV)	T1_ADC2(eV)	f01_ADC2(au)
count	12879.000000	12879.000000	12879.000000	12879.000000	12879.000000	12879.000000	12879.000000
mean	14.412144	6.287543	4.989370	0.099150	6.080681	5.009070	0.085172
std	2.907145	1.220643	1.372904	0.218265	1.196321	1.277183	0.169825
min	2.000000	1.809000	0.957000	0.000000	1.708240	0.945684	0.000000
25%	12.000000	5.657500	4.038000	0.001136	5.465241	4.093702	0.001144
50%	14.000000	6.393000	4.568000	0.007151	6.189377	4.732365	0.010504
75%	16.000000	7.011000	5.616000	0.050613	6.818060	5.924219	0.073313
max	23.000000	14.339000	13.844000	1.785412	14.010585	13.599737	1.362576

```
[2]: df.columns

Index(['SMI', 'Natoms', 'atoms', 'coords(Ang)', 'S1_SCSPEQIDH(eV)',
      'T1_SCSPEQIDH(eV)', 'f01_SCSPEQIDH(au)', 'S1_ADC2(eV)', 'T1_ADC2(eV)',
      'f01_ADC2(au)'],
      dtype='object')
```

Figure S3: Example query 1: Import the module `pymoldis` in Python code, load the `bigQM7 ω` dataset and perform a simple query to get an overall summary of the dataset using `.describe()` and the names of all the columns using the `columns` functionalities of `Pandas` module. Screenshot of a Jupyter notebook available at <https://github.com/moldis-group/pymoldis>. Note that, in `pymoldis`, we have removed the entries for the O_2 molecule as it is stable as a triplet in its ground state.


```
[1]: import pymoldis
import pandas as pd

df=pymoldis.get_data('bigqm7w_S1T1')
```

```
[2]: diff_S1=df['S1_SCS-PBE-QIDH(eV)']-df['S1_ADC2(eV)']
diff_T1=df['T1_SCS-PBE-QIDH(eV)']-df['T1_ADC2(eV)']
diff_S1T1=(df['S1_SCS-PBE-QIDH(eV)']-df['T1_SCS-PBE-QIDH(eV)'])-(df['S1_ADC2(eV)'] -df['T1_ADC2(eV)'] )
```

```
[3]: diff=pd.concat([diff_S1, diff_T1, diff_S1T1],axis=1)
diff.columns=['Delta S1 (DFT-ADC2) (eV)','Delta T1(DFT-ADC2) (eV)','Delta S1T1 (DFT-ADC2) (eV)']
diff.describe()
```

```
[3]:
```

	Delta S1 (DFT-ADC2) (eV)	Delta T1(DFT-ADC2) (eV)	Delta S1T1 (DFT-ADC2) (eV)
count	12879.000000	12879.000000	12879.000000
mean	0.206861	-0.019700	0.226561
std	0.170101	0.199748	0.196457
min	-0.383320	-0.746130	-0.249989
25%	0.109476	-0.158107	0.069795
50%	0.200098	-0.053379	0.211206
75%	0.302947	0.087925	0.354126
max	1.039420	0.931055	1.295653

Figure S4: Example query 2: Import `pymoldis`, calculate the deviations of SCS-PBE-QIDH predictions from ADC(2) values of S_1 , T_1 , and S_1-T_1 energies, and get a summary of all three deviations.

```
[1]: import pymoldis
import matplotlib.pyplot as plt

df=pymoldis.get_data('bigqm7w_S1T1')
```

```
[2]: s1=df['S1_ADC2(eV)']
t1=df['T1_ADC2(eV)']
stg_adc2=s1-t1
```

```
[3]: s1=df['S1_SCS-PBE-QIDH(eV)']
t1=df['T1_SCS-PBE-QIDH(eV)']
stg_dft=s1-t1
```

```
[4]: plt.scatter(stg_adc2, stg_dft)
plt.xlabel('$S_1-T_1$ from ADC(2) (eV)')
plt.ylabel('$S_1-T_1$ from SCS-PBE-QIDH (eV)')
plt.title('Scatter plot')
plt.show()
```

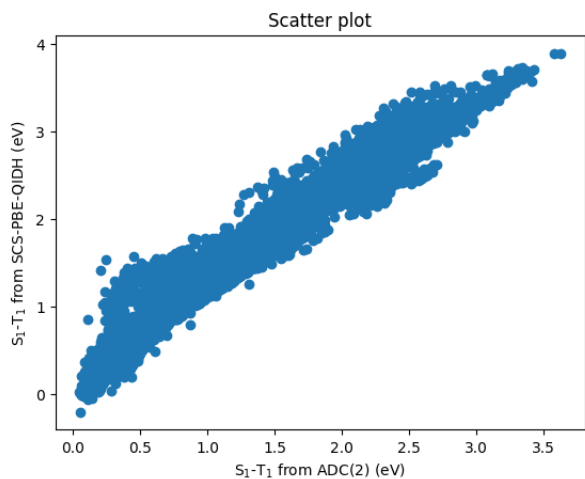


Figure S5: Example query 3: Import `pymoldis`, load S_1-T_1 energies from the SCS-PBE-QIDH and ADC(2) methods, and make a scatterplot.

```
[1]: import pymoldis
import pandas as pd

df=pymoldis.get_data('bigqm7w_S1T1')

S1T1_DFT=df['S1_SCSQBQIDH(eV)'] - df['T1_SCSQBQIDH(eV)']

NEntries=15

SmallGap_DFT_vals=S1T1_DFT.nsmallest(NEntries)

SMIs=df.iloc[SmallGap_DFT_vals.index]['SMI']

result = pd.concat([SMIs, SmallGap_DFT_vals], axis=1)
result.columns = ['SMI','S1-T1(eV)']
print(result)
```

	SMI	S1-T1(eV)
2674	'CC1(C)OC1(C)C'	-0.199
6449	'CCC1(C)CN1C'	-0.054
9153	'OC1CC2CN2C1'	-0.046
900	'CN1CC1(C)C'	-0.024
12679	'CC1CCC2CN12'	-0.019
9675	'CCC1(CF)CC1'	-0.012
12783	'CC1C2CN1C2'	-0.008
12675	'CC1CCN2CC12'	-0.003
899	'CC1OC1(C)C'	0.007
6451	'CN1CC1(C)CO'	0.011
2232	'C1CN2CC1C2'	0.012
9204	'CC1CC2CN1C2'	0.017
3692	'CCN1CC1(C)C'	0.023
2154	'CCC1CN1C'	0.028
9122	'C1CC2CN(C1)C2'	0.028

Figure S6: Example query 4: Find 15 molecules in the bigQM7 ω dataset with the smallest S_1 - T_1 energy gaps according to the SCS-PBE-QIDH/def2-TZVP method.

```
[1]: import pymoldis
import pandas as pd

df=pymoldis.get_data('bigqm7w_S1T1')
```

Find molecules with the least S1-T1 gap in DFT and ADC2

```
[2]: diff_dft=df['S1_SCSQBQIDH(eV)'] - df['T1_SCSQBQIDH(eV)']
diff_adc2=df['S1_ADC2(eV)'] - df['T1_ADC2(eV)']

N_smallest=5
entries_dft=df.iloc[diff_dft.abs().nsmallest(N_smallest).index]
entries_adc2=df.iloc[diff_adc2.abs().nsmallest(N_smallest).index]
```

Union of both sets

```
[3]: union_df=pd.concat([entries_dft, entries_adc2]).drop_duplicates()
print(union_df[['SMI']])
```

	SMI
12675	'CC1CCN2CC12'
899	'CC10C1(C)C'
12783	'CC1C2CCN1C2'
6451	'CN1CC1(C)CO'
2232	'C1CN2CC1C2'
12810	'C1C2CC3C1N3C2'
2674	'CC1(C)OC1(C)C'
9204	'CC1CC2CN1C2'
9151	'CC1CC2CN2C1'

Intersection of both sets

```
[4]: intersection_df=pd.merge(entries_dft, entries_adc2, how='inner')
print(intersection_df[['SMI']])
```

	SMI
0	'C1CN2CC1C2'

Figure S7: Example query 5: Find 5 molecules in the bigQM7 ω dataset with the smallest S₁-T₁ energy gaps according to the SCS-PBE-QIDH/def2-TZVP and the ADC(2) methods. Then, find the union and intersection of both sets.

```
[1]: import pymoldis

df=pymoldis.get_data('bigqm7w_S1T1')
```

```
[2]: index=2232
xyzfile='Mol_002232.xyz' # The XYZ will also be stored in this file
pymoldis.makexyz(index,df,xyzfile)
```

```
15
Mol_002232.xyz
C 1.16551200 0.75720200 -0.00000400
C 1.07023400 -0.80010900 0.00000300
N -0.39240300 -1.04289800 0.00000500
C -0.82255300 -0.01894200 1.01610000
C -0.33864800 1.03267300 -0.00000400
C -0.82255400 -0.01895100 -1.01609900
H 1.66444500 1.15390500 -0.88491300
H 1.66444600 1.15391200 0.88490200
H 1.51620400 -1.25541900 0.88379500
H 1.51620300 -1.25542600 -0.88378600
H -0.32334700 -0.08922200 1.98477500
H -1.90392100 -0.04919600 1.14389800
H -0.67188200 2.06893800 -0.00000900
H -0.32334800 -0.08923900 -1.98477400
H -1.90392200 -0.04920600 -1.14389600
```

Figure S8: Example query 6: Get the Cartesian coordinates of the equilibrium geometry of a molecule in the bigQM7 ω dataset (determined at the ω B97-XD/def2-TZVP level) using an index (perhaps one of them from the queries shown in Figure S6 or Figure S7.).

```
[1]: import pymoldis

df=pymoldis.get_data('bigqm7w_S1T1')

lower_bound=2.5
upper_bound=3.0

filtered_df=df[(df['S1_ADC2(eV)'] >= lower_bound) & (df['S1_ADC2(eV)'] <= upper_bound) &
               (df['T1_ADC2(eV)'] >= lower_bound) & (df['T1_ADC2(eV)'] <= upper_bound)]

filtered_df=filtered_df[['SMI', 'S1_ADC2(eV)', 'T1_ADC2(eV)', 'f01_ADC2(au)']]

print(filtered_df.describe())
```

	S1_ADC2(eV)	T1_ADC2(eV)	f01_ADC2(au)
count	29.000000	29.000000	29.000000
mean	2.917751	2.554014	0.000651
std	0.046181	0.058709	0.001818
min	2.806677	2.501329	0.000000
25%	2.882445	2.509465	0.000070
50%	2.925369	2.530179	0.000166
75%	2.952525	2.572719	0.000287
max	2.984915	2.712730	0.009470

```
[2]: #uncomment the next line to see the full list
#filtered_df
```

Figure S9: Example query 7: Find molecules with S_1 and T_1 energies in the range 2.5–3.0 eV, and print a summary.

```
[1]: import pymoldis

df=pymoldis.get_data('bigqm7w_S1T1')

sorted_osc_str=df.sort_values(by='f01_SCSPEQIDH(au)', ascending=False)
filtered_values=sorted_osc_str[sorted_osc_str['S1_SCSPEQIDH(eV)'] <= 3]

print(filtered_values[['SMI', 'S1_SCSPEQIDH(eV)', 'T1_SCSPEQIDH(eV)', 'f01_SCSPEQIDH(au)']].head(10))
```

	SMI	S1_SCSPEQIDH(eV)	T1_SCSPEQIDH(eV)	f01_SCSPEQIDH(au)
12464	'N1C=CN=NC=N1'	2.677	1.835	0.012447
2283	'c1nncnn1'	2.513	1.831	0.009638
7830	'Oc1nncnn1'	2.528	1.863	0.009556
7829	'Nc1nncnn1'	2.532	1.874	0.009373
7828	'Cc1nncnn1'	2.456	1.789	0.009014
7650	'N=c1nncn[nH]1'	2.636	1.894	0.006721
7674	'N=c1nncnol'	2.561	1.813	0.005766
7666	'N=c1nnccol'	2.939	2.144	0.005710
7651	'O=c1nncn[nH]1'	2.366	1.672	0.005283
7675	'O=c1nncnol'	2.290	1.578	0.004827

Figure S10: Example query 8: Find the bigQM7 ω molecules with the largest oscillator strength for the $S_0 \rightarrow S_1$ excitation, and print entries corresponding to the excitation energy of the S_1 state ≤ 3 eV.

```
[1]: import pymoldis
df=pymoldis.get_data('bigqm7w_S1T1')
```

```
[2]: pymoldis.print_MolFormula(df) # to print all molecular formulas in the dataset
```

```
Item: C5_H9_N1_01, Frequency: 319
Item: C4_H8_N2_01, Frequency: 295
Item: C6_H10_01, Frequency: 293
Item: C5_H11_N1_01, Frequency: 287
Item: C4_H6_N2_01, Frequency: 262
Item: C5_H8_02, Frequency: 255
Item: C5_H7_N1_01, Frequency: 239
Item: C6_H11_N1, Frequency: 236
Item: C6_H8_01, Frequency: 236
Item: C5_H8_N2, Frequency: 222
Item: C5_H10_N2, Frequency: 222
Item: C4_H7_N1_02, Frequency: 207
Item: C6_H13_N1, Frequency: 197
Item: C6_H12_01, Frequency: 193
Item: C5_F1_H9_01, Frequency: 189
Item: C5_H10_02, Frequency: 188
Item: C6_H9_N1, Frequency: 177
Item: C4_H10_N2_01, Frequency: 176
```

```
[3]: Formula='C3_H4_O4' # pick a molecular formula
indices=pymoldis.get_ConstitutionalIsomers(df,Formula) # get the indices of the constitutional isomers for the formula
indices
```

```
[3]: [2561, 3104, 5980, 6029, 7426, 9915]
```

```
[4]: print(df[['SMI', 'S1_SCSPEQIDH(eV)', 'S1_ADC2(eV)']].iloc[indices]) # get the properties of interest
```

	SMI	S1_SCSPEQIDH(eV)	S1_ADC2(eV)
2561	'OC(=O)CC(O)=O'	5.956	5.845653
3104	'OC(=O)COC=O'	6.013	5.933349
5980	'OCC(=O)C(O)=O'	3.768	3.651278
6029	'COC(=O)C(O)=O'	4.498	4.358432
7426	'O=C1OCOC1'	7.023	6.928801
9915	'O=COCOC=O'	5.926	5.845559

Figure S11: Example query 9: Get a list of all molecular formula (atomic compositions) spanned by the bigQM7w molecules. Pick a molecular formula, and for the corresponding constitutional isomers, get indices, SMILES, and energetics.

```
[1]: import pymoldis  
df=pymoldis.get_data('bigqm7w_S1T1')
```

```
[2]: def svg_from_smiles(SMI):  
  
    from rdkit import Chem  
    from rdkit.Chem import Draw  
    from rdkit.Chem.Draw import rdMolDraw2D  
    from io import StringIO  
  
    mol=Chem.MolFromSmiles(SMI)  
    drawer=rdMolDraw2D.MolDraw2DSVG(300, 300)  
    drawer.DrawMolecule(mol)  
    drawer.FinishDrawing()  
    svg=drawer.GetDrawingText()  
  
    return svg
```

```
[3]: from IPython.display import SVG  
  
index=2232  
smiles=(df.iloc[index]['SMI']).strip("")  
print(smiles)  
image=svg_from_smiles(smiles)  
SVG(image)  
C1CN2CC1C2
```

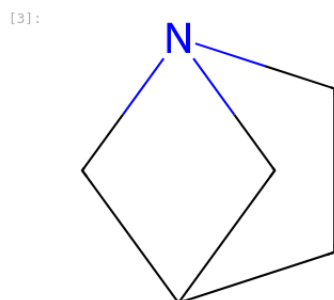


Figure S12: Example query 10: For an index in the bigQM7 ω dataset, get the corresponding SMILES, and visualize the cartoon representation using the rdkit module

MINIMUM ENERGY COORDINATES (ANGSTROEM) OF STRUCTURE 1 IN FIGURE 6
Calculated with wB97X-D3/def2-TZVP

N	0.390872	1.428585	1.624955
C	0.708861	1.815707	0.253755
C	0.575682	3.347565	0.045517
C	0.089341	3.961412	1.361490
H	-0.131796	3.573618	-0.756278
H	1.533710	3.788806	-0.241382
C	1.283999	2.122298	2.548251
C	1.118564	3.662217	2.456078
H	0.778668	4.076750	3.408734
H	2.070037	4.145241	2.219926
H	1.071210	1.764467	3.558078
C	-0.992622	1.786176	1.923318
C	-1.241399	3.307219	1.744630
H	-0.039013	5.039944	1.249580
H	-1.985937	3.494278	0.966417
H	-1.626810	3.750993	2.666145
H	1.723467	1.477122	0.032424
H	-1.642047	1.200697	1.268645
H	-1.207181	1.472821	2.947557
H	2.307905	1.823158	2.312964
H	0.038048	1.268226	-0.412274

MINIMUM ENERGY COORDINATES (ANGSTROEM) OF STRUCTURE 2 IN FIGURE 6
Calculated with wB97X-D3/def2-TZVP

N	0.059194	1.259689	-0.034749
C	0.181223	1.369404	-1.395803
C	-0.296127	2.902657	-1.396472
C	0.054220	3.314306	0.129364
H	-1.363092	3.048798	-1.581413
H	0.243182	3.522982	-2.117687
C	1.181099	1.199343	0.750894
C	1.520318	2.753136	0.525266
H	1.915932	3.242972	1.419373
H	2.223629	2.952868	-0.286825
C	1.528474	-0.295853	0.278838
H	0.899558	1.113411	1.801396
C	-1.183797	1.210035	0.541175
C	-1.055725	2.697881	1.134222
H	0.050930	4.414046	0.217821
H	-1.993011	3.260095	1.099742
H	-0.688225	2.748816	2.162011
C	-0.289605	-0.146435	-1.640642
H	1.235079	1.394086	-1.677194
C	0.064753	-0.795176	-0.200259
H	0.247777	-0.642054	-2.453944
H	-1.356951	-0.264126	-1.843230
H	1.929624	-0.922619	1.080084
H	2.228482	-0.357077	-0.558021
C	-1.048484	-0.352316	0.888450
H	0.066962	-1.894859	-0.288843
H	-1.956302	1.270798	-0.226817
H	-0.683096	-0.565357	1.895970
H	-1.983093	-0.906070	0.762965

MINIMUM ENERGY COORDINATES (ANGSTROM) OF STRUCTURE 3 IN FIGURE 6
Calculated with wB97X-D3/def2-TZVP

N	0.379208	1.545025	1.615145
C	0.522414	1.919464	0.194214
C	0.040684	3.378560	-0.020385
C	0.070623	4.079408	1.341912
H	-0.971796	3.397890	-0.435621
H	0.687101	3.882379	-0.742271
C	1.397206	2.264418	2.406877
C	1.412052	3.764525	2.012063
H	1.569465	4.382515	2.898662
H	2.237474	3.978652	1.325930
H	1.089246	2.185002	3.450570
C	-0.962585	1.942004	2.086010
C	-1.045306	3.486323	2.208089
H	-0.060595	5.156597	1.225223
H	-2.028676	3.834363	1.884747
H	-0.923759	3.801422	3.249156
H	1.589067	1.872414	-0.031392
H	-1.668148	1.617693	1.319548
C	-1.351177	1.237061	3.350943
C	-2.472023	0.550734	3.501386
H	-0.672436	1.330637	4.194999
H	-3.177772	0.431281	2.685513
H	-2.727656	0.079541	4.442427
C	2.748725	1.623174	2.311812
C	3.451742	1.226245	3.359832
H	3.172792	1.510693	1.317038
H	4.436513	0.788344	3.252706
H	3.063378	1.320067	4.368993
C	-0.151387	0.943751	-0.723295
C	0.442594	0.367902	-1.755661
H	-1.200067	0.730826	-0.531445
H	-0.090516	-0.308915	-2.411831
H	1.487653	0.552956	-1.982883

MINIMUM ENERGY COORDINATES (ANGSTROEM) OF STRUCTURE 4 IN FIGURE 6
Calculated with wB97X-D3/def2-TZVP

N	0.355841	1.689193	1.598935
C	0.654217	1.567608	0.241850
C	0.916390	3.184956	0.110907
C	0.117101	3.739458	1.383964
H	0.492086	3.569881	-0.818793
H	1.953136	3.517290	0.137921
C	1.382307	1.891585	2.521578
C	0.949315	3.463932	2.724722
H	0.351171	3.699694	3.603907
H	1.834938	4.101303	2.773002
C	1.206907	0.380433	3.106052
C	-0.962678	1.564839	2.037086
C	-1.333716	3.064287	1.474371
H	-0.010959	4.829075	1.268782
H	-1.838994	3.113681	0.510825
H	-1.969501	3.596206	2.185549
C	1.368005	0.121696	0.488440
C	0.595592	-0.357605	1.814591
H	2.440757	0.147130	0.671914
H	1.195988	-0.565099	-0.340160
H	0.525997	0.275976	3.949162
H	2.159615	-0.058002	3.402458
C	-0.972163	-0.025668	1.682064
H	0.723680	-1.446292	1.930783
H	-1.563157	-0.604598	2.391255
H	-1.320345	-0.286401	0.684087
C	-1.319803	1.664616	3.508357
C	-2.446498	1.175892	4.005664
H	-0.689579	2.244579	4.167756
H	-3.139819	0.593203	3.409219
H	-2.718670	1.354144	5.037962
C	2.830237	1.995063	2.078788
C	3.843275	1.830891	2.916769
H	3.056792	2.300071	1.066856
H	4.862687	2.000213	2.594920
H	3.698317	1.535684	3.950444
C	-0.433615	1.319396	-0.787093
C	-0.169445	0.856936	-2.000303
H	-1.452131	1.607214	-0.567215
H	-0.950220	0.771167	-2.744907
H	0.828234	0.554823	-2.300199

References

- (1) Loos, P.-F.; Lipparini, F.; Jacquemin, D. Heptazine, Cyclazine, and Related Compounds: Chemically-Accurate Estimates of the Inverted Singlet–Triplet Gap. *J. Phys. Chem. Lett.* **2023**, *14*, 11069–11075.
- (2) Curtis, K.; King, C.; Odoh, S. O. Novel Triangulenes: Computational Investigations of Energy Thresholds for Photocatalytic Water Splitting. *ChemPhysChem.* **2023**, *24*, e202300556.